Structural, magnetic, thermal, and electronic transport properties of single-crystal $EuPd_2Sb_2$

S. Das,[1] K. McFadden,[1] Yogesh Singh,[1] R. Nath,[1] A. Ellern,[2] and D. C. Johnston[1]
[1]*Ames Laboratory and Department of Physics and Astronomy, Iowa State University, Ames, Iowa 50011, USA*
[2]*Department of Chemistry, Iowa State University, Ames, Iowa 50011, USA*
(Received 7 December 2009; revised manuscript received 6 January 2010; published 17 February 2010)

Single crystals of $EuPd_2Sb_2$ have been grown from PdSb self-flux. The properties of the single crystals have been investigated by x-ray diffraction, magnetic susceptibility χ, magnetization M, electrical resistivity ρ, Hall coefficient R_H, and heat capacity C_p measurements versus temperature T and magnetic field H. Single-crystal x-ray diffraction studies confirmed that $EuPd_2Sb_2$ crystallizes in the tetragonal $CaBe_2Ge_2$-type structure. The $\chi(T)$ measurements suggest antiferromagnetic ordering at 6.0 K with the easy axis or plane in the crystallographic *ab* plane. An additional transition occurs at 4.5 K that may be a spin reorientation transition. The $C_p(T)$ data also show the two transitions at 6.1 and 4.4 K, respectively, indicating the bulk nature of the transitions. The 4.4 K transition is suppressed below 1.8 K while the 6.1 K transition moves down to 3.3 K in $H=8$ T. The $\rho(T)$ data show metallic behavior down to 1.8 K along with an anomaly at 5.5 K in zero field. The anomaly is suppressed to 2.7 K in an 8 T field. The R_H measurements indicated that the dominant charge carriers are electrons. The $M(H)$ isotherms show three field-induced transitions at 2.75, 3.90, and 4.2 T magnetic fields parallel to the *ab* plane at 1.8 K. No transitions are observed in $M(H)$ for fields parallel to the *c* axis.

DOI: 10.1103/PhysRevB.81.054425 PACS number(s): 75.50.Ee, 75.40.Cx, 71.20.Be, 75.30.Kz

I. INTRODUCTION

The recent discovery of high-temperature superconductivity in $RFeAsO_{1-x}F_x$ (R=La, Ce, Pr, Nd, Sm, Gd, Tb, and Dy)[1–6] compounds with superconducting transition temperatures T_c as high as 55 K has sparked a lot of interest in the search for new superconductors. These materials crystallize in the tetragonal ZrCuSiAs-type structure with space group $P4/nmm$.[7] The structure consists of alternating FeAs and RO layers stacked along the crystallographic *c* axis. The parent compounds RFeAsO exhibit spin density wave (SDW) transitions at temperatures $\lesssim$200 K.[3,8,9] Upon doping with F, the SDW is suppressed and superconductivity appears.[2–6,8,10]

Another group of structurally related parent compounds with the chemical formula AFe_2As_2 (A=Ca, Sr, Ba, and Eu) was soon discovered to show superconductivity upon doping or application of pressure. These compounds crystallize in the tetragonal $ThCr_2Si_2$-type structure with space group $I4/mmm$ (No. 139). The structure consists of alternating FeAs and A layers stacked along the *c* axis as shown in Fig. 1(a). In the FeAs layers, the Fe atoms form a square planar lattice. The AFe_2As_2 compounds also show SDW and structural transitions at high temperatures[11–20] which are suppressed by doping with K, Na, and Cs at the A site and accompanied by the onset of superconductivity.[21–24]

In both classes of $RFeAsO_{1-x}F_x$ and AFe_2As_2 compounds described above, FeAs layers that are stacked along the *c* axis are evidently a key building block yielding superconductors with relatively high T_c. This gives a strong motivation to investigate similarly structured compounds in a search for additional high-T_c superconductors.

The compound $EuPd_2Sb_2$ crystallizes in the $CaBe_2Ge_2$-type structure with space group $P4/nmm$ (No. 129),[25] as shown in Fig. 1(b). The structure is closely related to the AFe_2As_2 structure. Alternating PdSb and Eu layers are stacked along the *c* axis, similar to the AFe_2As_2 structure. However, there is a distinct difference between the two structures. In half of the PdSb layers in the $EuPd_2Sb_2$ structure, the Pd atoms are arranged in a square planar lattice with two Sb layers on either side of each Pd layer, resulting in a tetrahedral coordination of Pd by Sb as in the FeAs-type layers. However, alternating with these layers are layers in which the Pd and Sb positions are switched, as shown in Fig. 1(b). There are no previous reports on the physical properties of $EuPd_2Sb_2$ to the best of our knowledge.

There have been reports of structural instabilities and antiferromagnetic ordering in some other compounds forming in the $CaBe_2Ge_2$-type structure. $UCu_{1.5}Sn_2$ orders antiferromagnetically at 110 K which is very high among uranium intermetallics.[26] $CePd_2Ga_2$ undergoes a tetragonal to monoclinic second-order structural transition at 125 K and orders antiferromagnetically at 2.3 K.[27] $LaPd_2Ga_2$ is superconducting below 1.9 K.[27] Eu was reported to be in a mixed valent state between Eu^{+2} (spin $S=7/2$) and Eu^{+3} (spin $S=0$) in polycrystalline samples of $EuPd_2Sb_2$.[25] In this paper, we report the synthesis and structure of single crystals of $EuPd_2Sb_2$ and their physical properties including magnetic susceptibility, magnetization, specific heat, and electronic transport measurements.

II. EXPERIMENTAL DETAILS

Single crystals of $EuPd_2Sb_2$ were grown using PdSb self-flux which melts at ~805 °C. The Eu (99.999% pure) was obtained from the Ames Laboratory Materials Preparation Center. The Pd (99.95% pure) and Sb (99.999% pure) were obtained from Alfa-Aesar. Pd and Sb powders were thoroughly mixed inside a helium-filled glovebox, and then poured on top of a chunk of Eu (~0.1 g) that was placed at the bottom of a 2 ml alumina crucible. The elements were in the atomic ratio Eu:Pd:Sb=1:5:5. The top of the crucible was packed with quartz wool. The crucible was then sealed in a quartz tube under vacuum and was placed vertically in a box furnace and heated to 1000 °C at a rate of 76 °C/h and

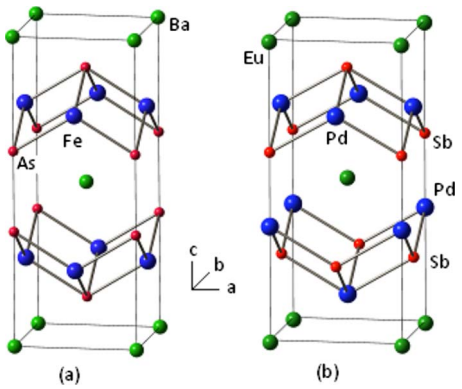

FIG. 1. (Color online) (a) Crystal structure of $BaFe_2As_2$ with the tetragonal $ThCr_2Si_2$-type structure. The structure consists of alternating FeAs and Ba layers stacked along the crystallographic *c* axis. (b) Crystal structure of $EuPd_2Sb_2$ with the origin of the unit cell shifted by (1/4 1/4 1/4) compared to that in the space group $P4/nmm$, for comparison purposes. The structure consists of alternating PdSb and Eu layers stacked along the crystallographic *c* axis similar to the $BaFe_2As_2$ shown in (a). However, half of the PdSb layers are inverted (the Pd and Sb atoms switch positions) with respect to the FeAs-type layers.

held there for 6 h. The tube was then cooled to 850 °C at the rate of 1.5 °C/h and at this temperature the tube was removed from the oven and centrifuged to partially separate the flux from the crystals. A single conglomerated chunk (about 0.4 g) was found in the crucible after removing the quartz wool. Platelike gold-colored crystals were isolated mechanically. The largest crystals had dimensions of $\sim 2 \times 2 \times 0.1$ mm^3. The crystals are brittle and are easily broken into smaller pieces. Figure 2 shows an as-grown crystal on a mm grid.

Single-crystal x-ray diffraction measurements were done using a Bruker CCD-1000 diffractometer with Mo K_α ($\lambda = 0.710\,73$ Å) radiation. Magnetic measurements on the crystals were carried out using a Quantum Design superconducting quantum interference device magnetometer in the temperature *T* range of 1.8–350 K and magnetic field *H* range of 0–5.5 T. Heat capacity, electrical resistivity, and

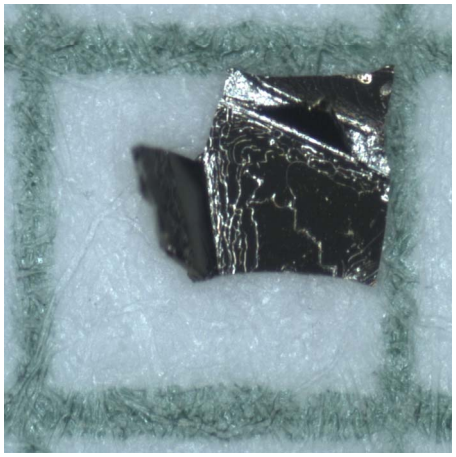

FIG. 2. (Color online) An as-grown crystal of $EuPd_2Sb_2$. The grid size in 1 mm.

TABLE I. Crystal data and structure refinement of $EuPd_2Sb_2$ at a temperature of 173 K. Here $R1 = \Sigma||F_{obs}| - |F_{calc}||/\Sigma|F_{obs}|$ and $wR2 = (\Sigma[w(|F_{obs}|^2 - |F_{calc}|^2)^2]/\Sigma[w(|F_{obs}|^2)^2])^{1/2}$, where F_{obs} is the observed structure factor and F_{calc} is the calculated structure factor.

Crystal system/space group	Tetragonal, $P4/nmm$
Unit cell parameters	$a = 4.653(2)$ Å
	$c = 10.627(4)$ Å
Unit cell volume	230.1(3) Å^3
Z (formula units/unit cell)	2
Density (Calculated)	8.779 Mg/m^3
Absorption coefficient	32.47 mm^{-1}
$F(000)$	514
Goodness-of-fit on F^2	1.235
Final *R* indices $[I > 2\sigma(I)]$	R1 = 0.0737
	wR2 = 0.02506
Extinction coefficient	0.033(9) mm^{-1}

Hall coefficient measurements were done using a Quantum Design physical property measurement system (PPMS). For the heat capacity measurements, Apiezon *N* grease was used for thermal coupling between a sample and the sample platform. The heat capacity was measured in the temperature range of 1.8–300 K in $H = 0$, 2, 5, 7, and 9 T. For electrical resistivity and Hall coefficient measurements, platinum leads were attached to the crystals using silver epoxy. Electrical resistivity measurements were carried out using the standard ac four probe method with 10 mA excitation current in the temperature range of 1.8–300 K and magnetic field range of 0–8 T. Hall coefficient measurements were carried out using the five-wire configuration supported by the PPMS ACT (Ref. 28) option with 100 mA excitation current in the temperature range of 1.8–310 K and magnetic field range of 0–8 T. The Hall voltage was computed at each temperature from the odd part of the measured transverse voltage upon reversing the sign of the applied magnetic field. The even part was much smaller than the odd part at each measured temperature.

III. RESULTS

A. Structure and chemical composition determination

A well-shaped crystal with dimensions of $0.21 \times 0.18 \times 0.11$ mm^3 was selected for single-crystal x-ray diffraction at 173 K. X-ray structure determination and refinement were performed using the SHELXTL software package.[29] The refined unit cell parameters, the isotropic thermal parameters, and the atomic positions are listed in Tables I and II. Our results confirm that $EuPd_2Sb_2$ crystallizes in the $CaBe_2Ge_2$ structure.[25] The unit cell dimensions and the atomic positions are similar to those found from single-crystal x-ray diffraction measurements at room temperature in Ref. 25, which were $a = 4.629(1)$ Å, $c = 10.568(2)$ Å, Eu: $z = 0.2424(1)$; Pd(2): $z = 0.6284(2)$; and Sb(2): $z = 0.8745(1)$. The significant difference between the lattice parameters in Ref. 25 and the lattice parameters obtained by us suggests a difference in

TABLE II. Atomic coordinates x, y, and z (10^{-4}) and equivalent isotropic displacement parameters U (10^{-3} Å^2) for $EuPd_2Sb_2$ at 173 K.

	x	y	z	U(eq)
Eu	2500	2500	2425(1)	13(1)
Pd(1)	7500	2500	0	16(1)
Pd(2)	2500	2500	6292(2)	17(1)
Sb(1)	7500	2500	5000	13(1)
Sb(2)	2500	2500	8738(1)	14(1)

crystal stoichiometry between the samples in Ref. 25 and ours, although both studies indicate nearly stoichiometric compositions. The temperature difference between the two studies cannot be responsible, since the lattice parameter differences are opposite to expectation in that case.

The stoichiometry of a representative crystal was checked by semiquantitative energy-dispersive x-ray (EDX) microanalysis. The results gave the following composition: Eu, 24.9 ± 1.1 wt %; Pd, 35.5 ± 0.8 wt %; and Sb, 39.7 ± 1.0 wt %. These values are consistent with the values calculated for the composition $EuPd_2Sb_2$: Eu, 24.98 wt %; Pd, 34.98 wt %; and Sb, 40.03 wt %.

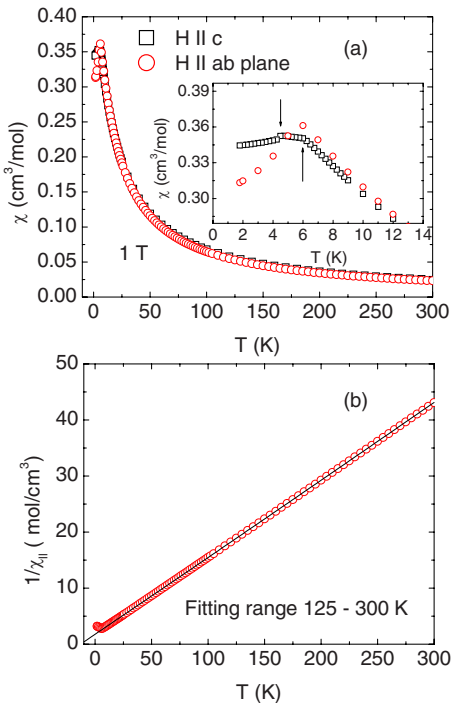

FIG. 3. (Color online) (a) Magnetic susceptibility χ versus temperature T of $EuPd_2Sb_2$ with the magnetic field H parallel to the crystallographic c axis and to the ab plane, respectively. The inset shows the low-T part of the $\chi(T)$ plot. The two transitions at 4.5 and 6.0 K are indicated by the vertical arrows. (b) Inverse susceptibility $1/\chi(T)$ for $H \| c$. The solid curve is the Curie-Weiss fit [Eq. (1)] to the $1/\chi_{\|}(T)$ data in the temperature range of 125–300 K with the parameters listed in the text.

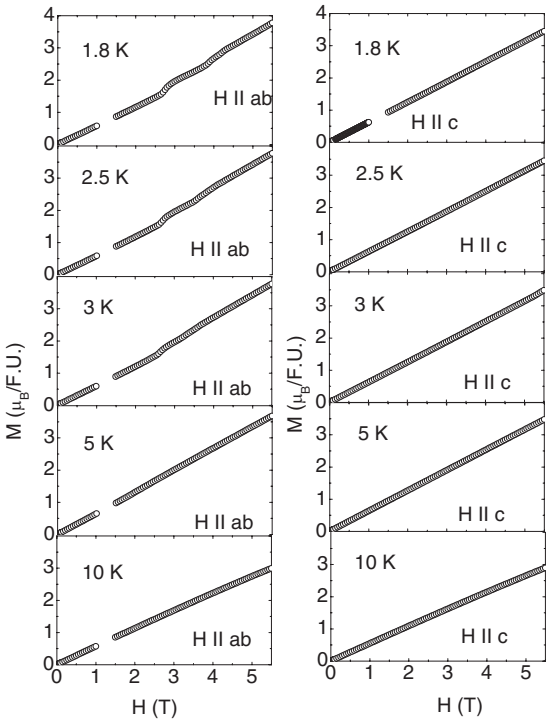

FIG. 4. Magnetization M versus applied magnetic field H of $EuPd_2Sb_2$ with H parallel to the crystallographic c axis (right-hand panels) and to the ab plane (left-hand panels), respectively.

B. Magnetic measurements

1. Magnetic susceptibility measurements

Figure 3(a) shows the magnetic susceptibility χ of $EuPd_2Sb_2$ versus temperature T with the magnetic field H parallel to the crystallographic c axis ($\chi_{\|}$) and to the ab plane ($\chi_{\perp}$), respectively. At high T, the $\chi(T)$ shows nearly isotropic paramagnetic behavior. Figure 3(b) shows the inverse susceptibility $1/\chi$ for $H \| c$ versus T. An excellent fit to the data in the T range of 125–300 K was obtained using the Curie-Weiss behavior

$$\frac{1}{\chi} = \frac{1}{\chi_0 + C/(T-\theta)}, \tag{1}$$

where χ_0 is the T-independent susceptibility, C is the Curie constant, and θ is the Weiss temperature. The values of the parameters obtained from the fit are $C = 7.333(8)$ cm^3 K/mol, $\theta = -12.9(2)$ K, and $\chi_0 = -0.00024(3)$ cm^3/mol. Keeping χ_0 fixed to zero, the Curie-Weiss fits to the $1/\chi_{\|}(T)$ data in different temperature ranges between 25–300 and 200–300 K yielded $C = 7.23(3)$ cm^3 K/mol and $\theta = -11.8(8)$ K. The obtained Curie constants are significantly lower than the value $C = 7.88$ cm^3 K/mol expected for Eu^{+2} (spin $S = 7/2$) with g factor $g = 2$. This indicates that Eu is in an intermediate valent state $Eu^{+2.07}$ as previously suggested in Ref. 25. The negative Weiss temperature indicates dominant antiferromagnetic interactions between the nearest-neighbor Eu spins.

At low temperatures, $\chi_{\|}$ becomes almost T independent below 6.0 K with a cusp at $T = 4.5$ K as shown in the inset of

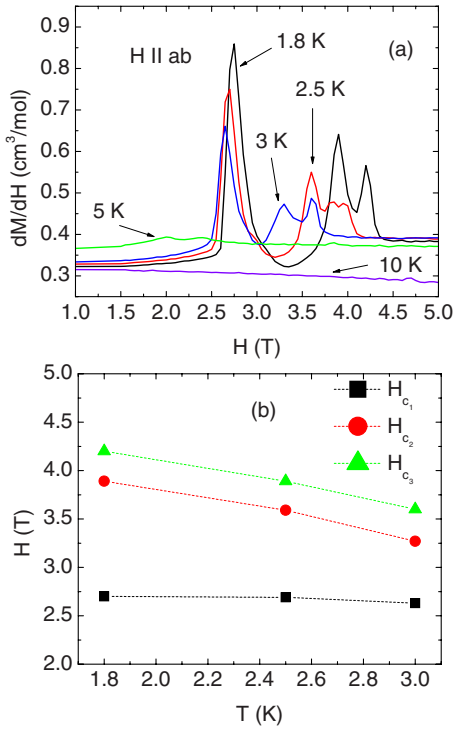

FIG. 5. (Color online) (a) Derivative dM/dH of the magnetization M with respect to the applied field H versus H with H parallel to the crystallographic ab plane. (b) The fields H_{c_1}, H_{c_2}, and H_{c_3}, at which transitions are observed in dM/dH, versus T. The dotted lines are guides to the eye.

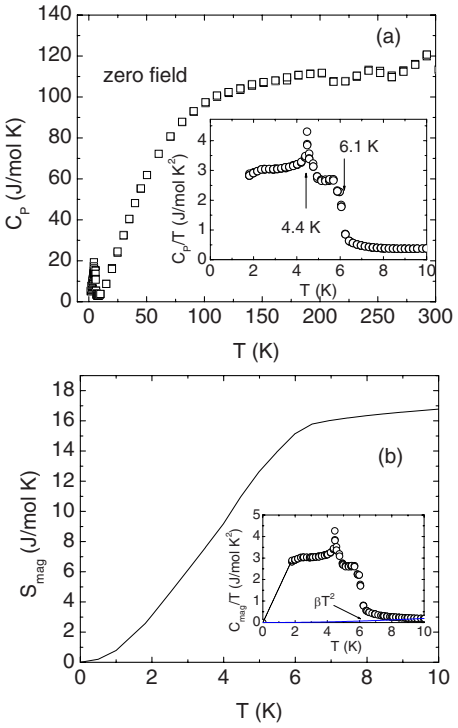

FIG. 6. (Color online) (a) Heat capacity C_p versus temperature T of $EuPd_2Sb_2$ in zero magnetic field. The inset shows C_p/T versus T for $T<10$ K. Two anomalies in $C_p(T)/T$ are observed at 4.4 and 6.1 K indicated by vertical arrows in the inset. (b) Calculated magnetic entropy $S_{mag}=\int_0^T[C_{mag}(T)/T]dT$ versus T. A linear extrapolation to zero of $C_p(T)/T$ as shown by the dotted straight line in the inset was used to approximate the missing C_p/T data between 0 and 1.8 K. The solid line in the inset is a plot of the lattice contribution $C_{latt}/T=\beta T^2$ with $\beta=1.92$ mJ/mol K^4 obtained for $BaRh_2As_2$ in Ref. 30. The inset shows that the lattice heat capacity is negligible compared to the magnetic heat capacity below 10 K.

Fig. 3(a). $\chi_\perp$ shows a peak at 6.0 K and decreases monotonically at lower T. The decrease in $\chi_\perp$ and almost constant $\chi_\parallel$ below 6 K suggest antiferromagnetic ordering of the Eu spins at $T_N=6.0$ K with the easy axis or plane within the ab plane. The cusp at 4.5 K in the $\chi_\parallel(T)$ data suggests a possible spin reorientation transition at 4.5 K. The small difference ($<10\%$) between $\chi_\parallel$ and $\chi_\perp$ and the high value of $\chi_\parallel$ at 1.8 K suggest a noncollinear arrangement of the Eu spins in the ab plane in the antiferromagnetically ordered state.

2. Magnetization versus applied magnetic field isotherm measurements

Figure 4 shows the magnetization M of $EuPd_2Sb_2$ versus magnetic field H with H parallel to the crystallographic c axis (right-hand panels) and to the ab plane (left-hand panels), respectively. For $H\|ab$, anomalies in $M(H)$ are clearly visible for $T<5$ K. Above 10 K, $M(H)$ is proportional to H. To illustrate the anomalies more clearly, Fig. 5(a) shows the derivative dM/dH versus H with $H\|ab$. The dM/dH data for $M\|ab$ show three peaks at $H_{c_1}=2.75$ T, $H_{c_2}=3.90$ T, and $H_{c_3}=4.20$ T, respectively, at 1.8 K. The temperature dependences of the fields at which these field-induced transitions occur are shown in Fig. 5(b). The transition fields are seen to decrease with increasing T, and disappear between 5 and 10 K. At 1.8 K in $H=5.5$ T, the value of $M\|ab$ in Fig. 4 is $3.8\mu_B$/f.u. This value is much less than the expected Eu^{+2} saturation moment of $7\mu_B$. This difference suggests that the metamagnetic transitions take place between different antiferromagnetic states. In contrast, $M\|c$ is proportional to H at all T.

C. Heat capacity measurements

Figure 6(a) shows the heat capacity C_p of a 2.619 mg $EuPd_2Sb_2$ crystal versus temperature T in zero magnetic field. The inset of Fig. 6(a) shows C_p/T versus T for $T<10$ K. Two anomalies are observed at 6.1 and 4.4 K, respectively, indicating that the transitions observed in $\chi(T)$ in the inset of Fig. 3(a) at similar temperatures are bulk long-range magnetic ordering transitions. The data at high $T\sim300$ K approach the Dulong-Petit classical lattice heat capacity value of $15R\simeq125$ J/mol K, where R is the molar gas constant.

Figure 6(b) shows the calculated magnetic entropy $S_{mag}=\int_0^T[C_{mag}(T)/T]dT$ versus T at low temperatures $T<10$ K, where $C_{mag}=C_p-C_{latt}$ is the magnetic contribution and C_{latt} is the lattice contribution to the specific heat. We assumed $C_{latt}=\beta T^3$ for $T<10$ K with $\beta=1.93(4)$ mJ/mol K^4 obtained for $BaRh_2As_2$ from Ref. 30. A linear extrapolation to $T=0$ of C_{mag}/T, as shown by the dotted straight line in the inset of Fig. 6(b), was assumed in order to approximate the

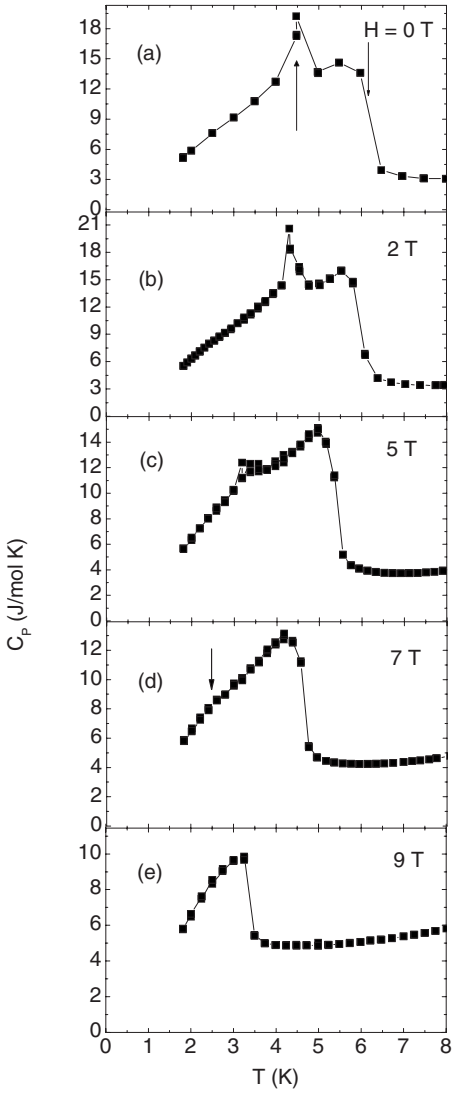

FIG. 7. Heat capacity C_p versus temperature T of $EuPd_2Sb_2$ in different magnetic fields parallel to the c axis. The two transitions at temperatures T_{N_1} and T_{N_2}, respectively, are indicated in panel (a). The vertical arrow in (d) points to T_{N_2} in $H=7$ T.

missing C_{mag}/T data between 0 and 1.8 K. The magnetic entropy $S_{mag}=16.7$ J/mol K at 10 K is close to the expected entropy $S_{mag}=R\ln(2S+1)=17.3$ J/mol K due to ordering of one spin $S=7/2$ per formula unit.

Figures 7(a)–7(e) show $C_p(T)$ in different magnetic fields parallel to the crystallographic c axis. For $H=0$ T, $C_p(T)$ shows a jump at $T_{N_1}=6.1$ K and then a cusp at $T_{N_1}=4.4$ K. The shapes of the C_p anomalies at the two transitions are thus distinctly different. As H is increased, T_{N_2} decreases below 1.8 K at 9 T, while the T_{N_1} goes down to 3.2 K in 9 T. The transition at T_{N_1} remains sharp while the transition at T_{N_2} broadens for $H>2$ T. Figure 8 shows plots of T_{N_1} and T_{N_2} versus H.

D. Electronic transport measurements

1. Electrical resistivity measurements

Figure 9 shows the electrical resistivity ratio ρ/ρ_{300} of $EuPd_2Sb_2$ for current parallel to the ab plane versus temperature T in 0 and 8 T magnetic fields parallel to the c axis, where ρ is the resistivity at temperature T and $\rho_{300}=(50\pm25)$ $\mu\Omega$ cm is the resistivity at 300 K. The large fractional uncertainty in ρ_{300} arises due to the uncertainty in the geometric factor for the irregularly shaped crystal. The inset shows the low-T region below 10 K. The resistivity data exhibit metallic behavior down to the lowest temperature. The residual resistivity ratio (RRR)$=\rho(300\text{ K})/\rho(2\text{ K})\approx10$. This value is comparable to the values found in the ab-plane resistivity for single crystals of other layered pnictides.[11,12,15,19] From the inset of Fig. 9, in zero magnetic field $\rho(T)$ shows a peak at 5.4 K which gets suppressed to 2.9 K in $H=8$ T. The anomaly is evidently due to the antiferromagnetic ordering at $T_{N_1}=6.1$ K at $H=0$ as observed from the $C_p(T)$ and $\chi(T)$ measurements.

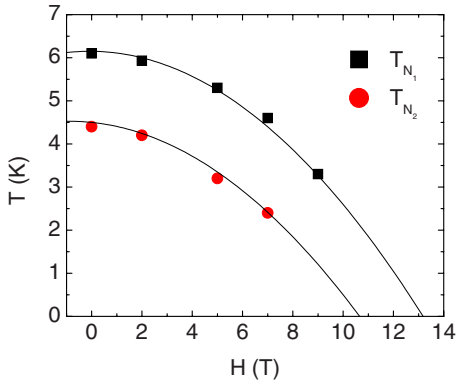

FIG. 8. (Color online) Transition temperatures T_{N_1} and T_{N_2} of $EuPd_2Sb_2$ versus magnetic field $H\|c$ as determined from the heat capacity measurements versus H in Fig. 7. The solid curves are guides to the eye.

2. Hall coefficient measurements

Figure 10(a) shows the Hall resistivity $\rho_H=V_HA/Il$ versus H, where V_H is the measured Hall voltage, A is the cross sectional area of the sample, l is the separation of the trans-

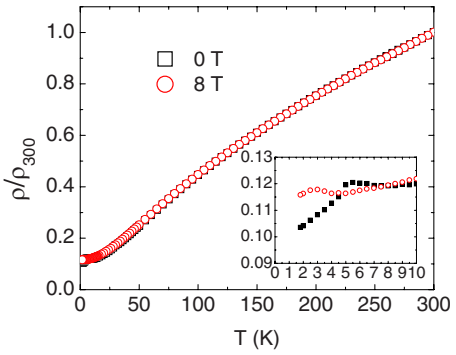

FIG. 9. (Color online) Electrical resistivity ratio ρ/ρ_{300} versus temperature T of $EuPd_2Sb_2$ for current in the ab plane in 0 and 8 T magnetic fields parallel to the c axis where ρ is the resistivity at temperature T and $\rho_{300}=(50\pm25)$ $\mu\Omega$ cm is the resistivity at 300 K. The inset shows the low-T region below 10 K, where the filled squares are the resistivity data for H=0 T and the open circles for H=8 T.

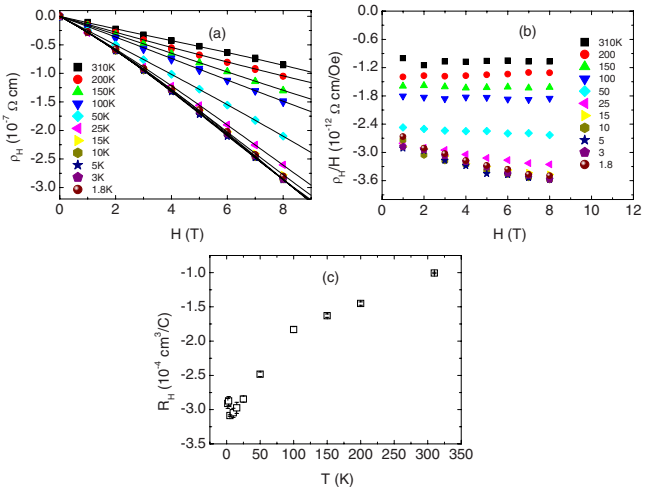

FIG. 10. (Color online) (a) Hall resistivity ρ_H of $EuPd_2Sb_2$ versus applied magnetic field H at the indicated temperatures T. The solid curves are polynomial fits to the data (see text). (b) ρ_H/H versus H at the indicated values of T. (c) Hall coefficient R_H versus T. The consistently negative R_H indicates that the dominant current carriers are electrons.

verse voltage leads, and I is the longitudinal current. In Fig. 10(a), ρ_H versus magnetic field H is seen to deviate from a proportional behavior below 100 K. This behavior is more clearly seen in the plot of ρ_H/H versus H in Fig. 10(b). The measured $\rho_H(H)$ data were fitted by the function $\rho_H(H) = a_1H + a_3H^3 + a_5H^5$, as shown by the solid curves in Fig. 10(a), where a_1 (the coefficient of the linear term) is the Hall coefficient R_H. R_H versus T is shown in Fig. 10(c), where R_H becomes more negative by a factor of 3 on cooling from 310 to 2 K. The temperature dependence is very similar to $R_H(T)$ of $BaRh_2As_2$ (Ref. 30) which crystallizes in the tetragonal $ThCr_2Si_2$-type structure. The consistently negative R_H indicates that the dominant charge carriers are electrons. If one uses a single band model, one obtains a conduction electron concentration $n=(R_He)^{-1}=7.2$ and 2.5 $(\text{f.u.})^{-1}$ at 310 and 2 K, respectively.

IV. SUMMARY AND DISCUSSION

We have synthesized single crystals of $EuPd_2Sb_2$ and characterized them using single-crystal x-ray diffraction, anisotropic magnetic susceptibility and magnetization, specific heat, electrical resistivity, and Hall coefficient measurements. The magnetic susceptibility indicates antiferromagnetic ordering at 6.0 K with an easy axis or plane within the crystallographic ab plane followed by another transition at 4.5 K. The transitions are also observed in heat capacity measurements indicating their bulk nature. The transition at 4.5 K is suppressed below 1.8 K in a magnetic field of 8 T as observed from the heat capacity and electrical resistivity measurements. The transition at 6 K is pushed down to 3.5 K in a field of 8 T. $M(H)$ isotherms show three field-induced transitions at 2.75, 3.90, and 4.2 T for magnetic fields parallel to the ab plane at 1.8 K. No transitions are observed for fields parallel to the c axis. Qualitatively similar $M(H)$ observations were previously reported for single crystals of $EuRh_2As_2$ (Ref. 31) and $EuFe_2As_2$,[32] where the Eu spins also order antiferromagnetically in the ab plane and metamagnetic transitions are observed only when $H \| ab$ plane.[31,32] The Hall coefficient is consistently negative from 1.8 to 310 K indicating electrons as the dominant charge carriers.

A comparison of structural and magnetic parameters of $EuPd_2Sb_2$ with those of some Eu compounds which form in the related $ThCr_2Si_2$-type structure is given in Table III.[19,31,33] Of the compounds listed in Table III, only $EuFe_2As_2$ shows superconducting behavior under pressure[34] as well as under doping at the Eu site.[23] T_N for $EuPd_2Sb_2$ with $a=4.653$ Å and a c/a ratio of 2.28 is 6.1 K compared to 20 K for $EuFe_2As_2$ which has a smaller $a=3.910$ Å and a much larger $c/a=3.10$. Thus the significant difference in T_N values is probably due at least in part to these structural differences. In $Eu_{0.5}K_{0.5}Fe_2As_2$ which is superconducting below 32 K,[23] however, AF ordering of the Eu spins still takes place below 10 K. The calculated effective moment of the Eu spins in $EuPd_2Sb_2$ is close to that of Eu spins in $EuFe_2As_2$. The Hall coefficient of $EuPd_2Sb_2$ remains negative between 1.8 and 300 K like that in the superconducting $Ba(Fe_{1-x}Co_x)_2As_2$ and $Ba(Fe_{1-x}Cu_x)_2As_2$.[35] However, in $EuFe_2As_2$, the Hall coefficient changes sign from negative to positive at ~175 K. At 300 K, $R_H \sim 0$ in $EuFe_2As_2$,[19] which suggests that the charge carriers comprise both electrons and holes.

The magnetic nature of the FeAs layers in $EuFe_2As_2$ is probably an important factor behind the superconducting behavior at high pressures.[34] The different structure of $EuPd_2Sb_2$ compared to the $ThCr_2Si_2$-type structure

TABLE III. A comparison of the structural and magnetic parameters of $EuPd_2Sb_2$ with some Eu compounds which form in the related $ThCr_2Si_2$-type structure. The structure type and the lattice parameters a and c are at room temperature for $EuFe_2As_2$ and $EuRh_2As_2$, at 124 K for $EuNi_2As_2$, and at 173 K for $EuPd_2Sb_2$. T_N is the antiferromagnetic ordering temperature and μ_{eff} is the effective moment in the Curie-Weiss law calculated from magnetic susceptibility measurements.

Compound	Structure type	a (Å)	c (Å)	T_N (K)	μ_{eff} (μ_B/f.u.)	Ref.
$EuFe_2As_2$	$ThCr_2Si_2$	3.9104	12.1362	20	7.79	19
$EuRh_2As_2$	$ThCr_2Si_2$	4.075	11.295	47		31
$EuNi_2As_2$	$ThCr_2Si_2$	4.0964	10.029	14		33
$EuPd_2Sb_2$	$CaBe_2Ge_2$	4.653	10.627	6.1	7.65	This work

might also contribute toward $EuPd_2Sb_2$ not being a superconductor. It will be very interesting to grow single crystals of $EuPd_{2-x}Fe_xSb_2$ and study their physical properties. The Fe doping at the Pd site will eventually make the Pd(Fe)-Sb layers structurally similar to the FeAs layers in $EuFe_2As_2$.

Note added. After submission of this paper for publication, we received a preprint describing related results on $EuPd_2Sb_2$.[36]

ACKNOWLEDGMENTS

Work at the Ames Laboratory was supported by the Department of Energy-Basic Energy Sciences under Contract No. DE-AC02-07CH11358.

[1] Y. Kamihara, T. Watanabe, M. Hirano, and H. Hosono, J. Am. Chem. Soc. **130**, 3296 (2008).
[2] X. H. Chen, T. Wu, G. Wu, R. H. Liu, H. Chen, and D. F. Fang, Nature (London) **453**, 761 (2008).
[3] G. F. Chen, Z. Li, D. Wu, G. Li, W. Z. Hu, J. Dong, P. Zheng, J. L. Luo, and N. L. Wang, Phys. Rev. Lett. **100**, 247002 (2008).
[4] Z.-A. Ren, J. Yang, W. Lu, W. Yi, X.-L. Shen, Z.-C. Li, G.-C. Che, X.-L. Dong, L.-L. Sun, F. Zhou, and Z.-X. Zhao, Europhys. Lett. **82**, 57002 (2008).
[5] J. Yang, Z.-C. Li, W. Lu, W. Yi, X.-L. Shen, Z.-A. Ren, G.-C. Che, X.-L. Dong, L.-L. Sun, F. Zhou, and X. Zhao, Supercond. Sci. Technol. **21**, 082001 (2008).
[6] J.-W. G. Bos, G. B. S. Penny, J. A. Rodgers, D. A. Sokolov, A. D. Huxley, and J. P. Attfield, Chem. Commun. (Cambridge) **2008**, 3634.
[7] P. Quebe, L. J. Terbuchte, and W. Jeitschko, J. Alloys Compd. **302**, 70 (2000).
[8] J. Dong, H. J. Zhang, G. Xu, Z. Li, G. Li, W. Z. Hu, D. Wu, G. F. Chen, X. Dai, J. L. Luo, Z. Fang, and N. L. Wang, Europhys. Lett. **83**, 27006 (2008).
[9] H.-H. Klauss, H. Luetkens, R. Klingeler, C. Hess, F. J. Litterst, M. Kraken, M. M. Korshunov, I. Eremin, S.-L. Drechsler, R. Khasanov, A. Amato, J. Hamann-Borrero, N. Leps, A. Kondrat, G. Behr, J. Werner, and B. Büchner, Phys. Rev. Lett. **101**, 077005 (2008).
[10] G. Giovannetti, S. Kumar, and J. van den Brink, Physica B **403**, 3653 (2008).
[11] M. Rotter, M. Tegel, D. Johrendt, I. Schellenberg, W. Hermes, and R. Pöttgen, Phys. Rev. B **78**, 020503(R) (2008).
[12] C. Krellner, N. Caroca-Canales, A. Jesche, H. Rosner, A. Ormeci, and C. Geibel, Phys. Rev. B **78**, 100504(R) (2008).
[13] N. Ni, S. L. Bud'ko, A. Kreyssig, S. Nandi, G. E. Rustan, A. I. Goldman, S. Gupta, J. D. Corbett, A. Kracher, and P. C. Canfield, Phys. Rev. B **78**, 014507 (2008).
[14] J.-Q. Yan, A. Kreyssig, S. Nandi, N. Ni, S. L. Bud'ko, A. Kracher, R. J. McQueeney, R. W. McCallum, T. A. Lograsso, A. I. Goldman, and P. C. Canfield, Phys. Rev. B **78**, 024516 (2008).
[15] N. Ni, S. Nandi, A. Kreyssig, A. I. Goldman, E. D. Mun, S. L. Bud'ko, and P. C. Canfield, Phys. Rev. B **78**, 014523 (2008).
[16] F. Ronning, T. Klimczuk, E. D. Bauer, H. Volz, and J. D. Thompson, J. Phys.: Condens. Matter **20**, 322201 (2008).
[17] A. I. Goldman, D. N. Argyriou, B. Ouladdiaf, T. Chatterji, A. Kreyssig, S. Nandi, N. Ni, S. L. Bud'ko, P. C. Canfield, and R. J. McQueeney, Phys. Rev. B **78**, 100506(R) (2008).
[18] M. Tegel, M. Rotter, V. Weiss, F. M. Schappacher, R. Pöttgen, and D. Johrendt, J. Phys. Condens.: Matter **20**, 452201 (2008).
[19] Z. Ren, Z. Zhu, S. Jiang, X. Xu, Q. Tao, C. Wang, C. Feng, G. Cao, and Z. Xu, Phys. Rev. B **78**, 052501 (2008).
[20] H. S. Jeevan, Z. Hossain, D. Kasinathan, H. Rosner, C. Geibel, and P. Gegenwart, Phys. Rev. B **78**, 052502 (2008).
[21] M. Rotter, M. Tegel, and D. Johrendt, Phys. Rev. Lett. **101**, 107006 (2008).
[22] G.-F. Chen, Z. Li, G. Li, W.-Z. Hu, J. Dong, J. Zhou, X.-D. Zhang, P. Zheng, N.-L. Wang, and J.-L. Luo, Chin. Phys. Lett. **25**, 3403 (2008).
[23] H. S. Jeevan, Z. Hossain, D. Kasinathan, H. Rosner, C. Geibel, and P. Gegenwart, Phys. Rev. B **78**, 092406 (2008).
[24] K. Sasmal, B. Lv, B. Lorenz, A. M. Guloy, F. Chen, Y. Y. Xue, and C. W. Chu, Phys. Rev. Lett. **101**, 107007 (2008).
[25] W. K. Hofmann and W. Jeitschko, Monatsh. Chem. **116**, 569 (1985).
[26] A. Purwanto, R. A. Robinson, H. Nakotte, I. P. Swainson and M. S. Torikachvili, J. Appl. Phys. **79**, 6411 (1996).
[27] J. Kitagawa and M. Ishikawa, J. Phys. Soc. Jpn. **68**, 2380 (1999).
[28] Quantum Design Physical Property Measurement System Manual.
[29] All software and sources of the scattering factors are contained in the SHELXTL (version 5.1) program library (G. Sheldrick, Bruker Analytical X-Ray Systems, Madison, WI).
[30] Y. Singh, Y. Lee, S. Nandi, A. Kreyssig, A. Ellern, S. Das, R. Nath, B. N. Harmon, A. I. Goldman, and D. C. Johnston, Phys. Rev. B **78**, 104512 (2008).
[31] Y. Singh, Y. Lee, B. N. Harmon, and D. C. Johnston, Phys. Rev. B **79**, 220401(R) (2009).
[32] S. Jiang, Y. Luo, Z. Ren, Z. Zhu, C. Wang, X. Xu, Q. Tao, G. Cao, and Z. Xu, New J. Phys. **11**, 025007 (2009).
[33] E. D. Bauer, F. Ronning, B. L. Scott, and J. D. Thompson, Phys. Rev. B **78**, 172504 (2008).
[34] T. Terashima, M. Kimata, H. Satsukawa, A. Harada, K. Hazama, S. Uji, H. S. Suzuki, T. Matsumoto, and K. Murata, J. Phys. Soc. Jpn. **78**, 083701 (2009).
[35] E. D. Mun, S. L. Bud'ko, Ni Ni, A. N. Thaler, and P. C. Canfield, Phys. Rev. B **80**, 054517 (2009).
[36] I. Schellenberg, M. Eul, and R. Pöttgen Z. Naturforsch., B: Chem. Sci. **65b**, 18 (2010).